Acta Cryst E CRYSTALLOGRAPHIC COMMUNICATIONS

ISSN 2056-9890

Crystal structure determination and analyses of Hirshfeld surface, crystal voids, intermolecular interaction energies and energy frameworks of 1-benzyl-4-(methylsulfanyl)-3a,7a-dihydro-1*H*-pyrazolo[3,4-*d*]pyrimidine

Received 16 May 2024
Accepted 19 June 2024

Edited by M. Weil, Vienna University of Technology, Austria

Keywords: crystal structure; pyrazolopyrimidine; sulfide; hydrogen bond; C—H···π(ring) interaction.

CCDC reference: 2363971

Supporting information: this article has supporting information at journals.iucr.org/e

Nour El Hoda Mustaphi,[a]* Amina Chlouchi,[a] Mohamed El Hafi,[b,c] Joel T. Mague,[d] Tuncer Hökelek,[e] Hanae El Monfalouti,[f] Amal Haoudi[g] and Ahmed Mazzah[h]

[a]Organic Chemistry, Catalysis and Environmental Laboratory, Higher National School of Chemistry, Ibn Tofail University Kenitra, Morocco, [b]Faculty of Medicine and Pharmacy, Mohammed First University, Oujda, Morocco, [c]Laboratory of Heterocyclic Organic Chemistry URAC 21, Pharmacochemistry Competence Center, Av. Ibn Battouta, BP 1014, Faculty of Sciences, Mohammed V University in Rabat, Morocco, [d]Department of Chemistry, Tulane University, New Orleans, LA 70118, USA, [e]Department of Physics, Hacettepe University, 06800 Beytepe, Ankara, Türkiye, [f]Laboratory of Plant Chemistry, Organic and Bioorganic Synthesis, Faculty of Sciences, Mohammed V University in Rabat, 4 Avenue Ibn Battouta, BP 1014 RP, Morocco, [g]Laboratory of Applied Organic Chemistry, Sidi Mohamed Ben Abdellah University, Faculty Of Science And Technology, Road Immouzer, BP 2202 Fez, Morocco, and [h]Science and Technology of Lille USR 3290, Villeneuve d'Ascq cedex, France. *Correspondence e-mail: nourelhoda.mustaphi@uit.ac.ma

The pyrazolopyrimidine moiety in the title molecule, $C_{13}H_{12}N_4S$, is planar with the methylsulfanyl substituent lying essentially in the same plane. The benzyl group is rotated well out of this plane by 73.64 (6)°, giving the molecule an approximate *L* shape. In the crystal, C—H···π(ring) interactions and C—H···S hydrogen bonds form tubes extending along the *a* axis. Furthermore, there are π–π interactions between parallel phenyl rings with centroid-to-centroid distances of 3.8418 (12) Å. A Hirshfeld surface analysis of the crystal structure indicates that the most important contributions to the crystal packing are from H···H (47.0%), H···N/N···H (17.6%) and H···C/C···H (17.0%) interactions. The volume of the crystal voids and the percentage of free space were calculated to be 76.45 Å^3 and 6.39%, showing that there is no large cavity in the crystal packing. Evaluation of the electrostatic, dispersion and total energy frameworks indicate that the cohesion of the crystal structure is dominated by the dispersion energy contributions.

1. Chemical context

The chemistry of heterocyclic compounds has attracted increasing interest in recent decades, driven by the therapeutic potential of many of these compounds, particularly those containing nitrogen. Notably, nitrogen heterocycles have emerged as promising candidates for bioactive molecules (Irrou *et al.*, 2022; Sebbar *et al.*, 2016). Among these, pyrazolo[3,4-*d*]pyrimidine stands out as an important compound, with its derivatives exhibiting various pharmacological properties (Severina *et al.*, 2016). They are widely used in pharmaceutical research for their anti-tumour (Kandeel *et al.*, 2012), anti-inflammatory (El-Tombary, 2013), antimicrobial (Bakavoli *et al.*, 2010), antioxidant (El-Mekabaty, 2015), anticonvulsant (Severina *et al.*, 2016) and anticancer (Maher *et al.*, 2019) properties. Additionally, pyrazolopyrimidines have been shown to treat Alzheimer's disease (Zhang *et al.*, 2018), human leukaemia (HL-60) (Song *et al.*, 2011) and exert potent activity against viruses of herpes (Gudmundsson *et al.*, 2009).

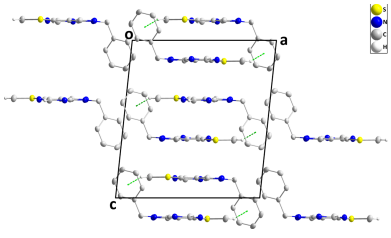

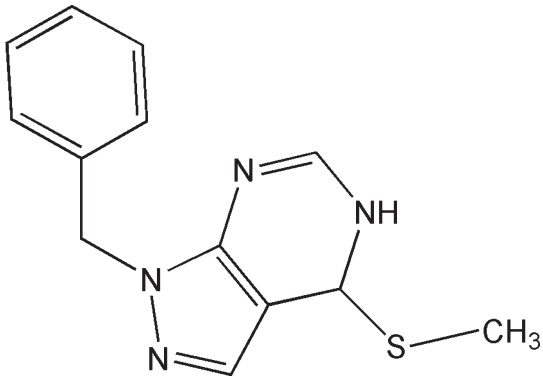

Continuing our research in this area, we synthesized the title compound, 1-benzyl-4-(methylsulfanyl)-3a,7a-dihydro-1*H*-pyrazolo[3,4-*d*]pyrimidine, (I), and carried out its crystal-structure determination, as well as analyses of the Hirshfeld surface, crystal voids, intermolecular interaction energies and energy frameworks.

2. Structural commentary

The pyrazolopyrimidine moiety of (I) is essentially planar (root-mean-square deviation = 0.0046 Å), and the C7–C12 phenyl ring is inclined to this plane by 73.64 (6)°, giving the molecule an approximate *L* shape (Fig. 1). The methylsulfanyl substituent lies in the mean plane of the pyrazolopyrimidine moiety, as indicated by the N1—C1—S1—C13 torsion angle of −0.32 (18)°. All bond lengths and angles in this molecule appear to be characteristic.

3. Supramolecular features

In the crystal of (I), inversion dimers are formed by C13—H13*C*···*Cg*3^{ii} interactions (*Cg*3 is the centroid of the C7–C12 phenyl ring). Through additional C—H···S hydrogen bonds, the dimers are connected into rectangular tubes extending parallel to the *a* axis (Table 1, Fig. 2). The tubes are stacked along the *c* axis by van der Waals contacts between them (Fig. 3). Furthermore, there are *Cg*3–*Cg*3^{i} interactions between parallel phenyl rings with a centroid-to-centroid distances of 3.8418 (12) Å [α = 0.03 (10)°; symmetry code: (i) $-x, -y, 1-z$].

Table 1
Hydrogen-bond geometry (Å, °).

*Cg*3 is the centroid of the C7–C12 phenyl ring.

D—H···*A*	*D*—H	H···*A*	*D*···*A*	*D*—H···*A*
C2—H2···S1^{i}	0.97 (3)	2.81 (3)	3.781 (2)	174 (2)
C13—H13*C*···*Cg*3^{ii}	1.02 (4)	2.49 (4)	3.455 (2)	157 (3)

Symmetry codes: (i) $x, y-1, z$; (ii) $-x+1, -y+1, -z+1$.

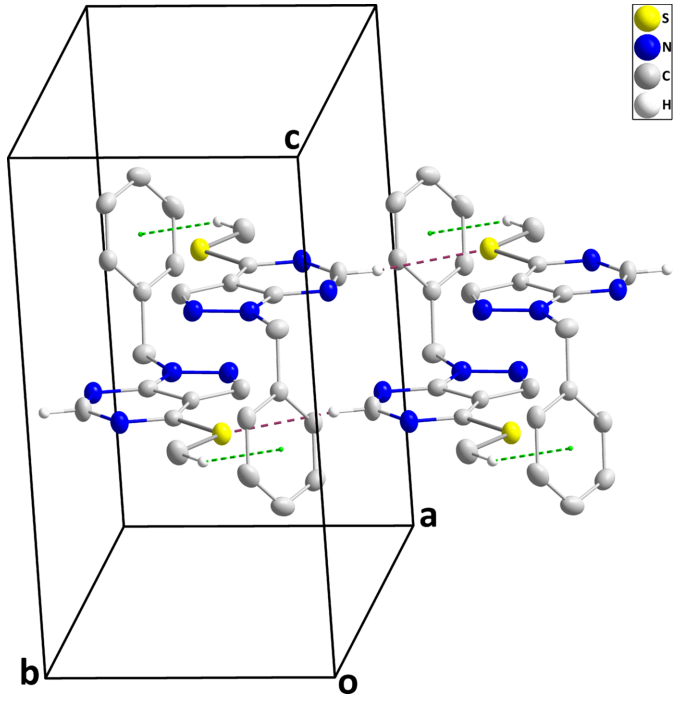

Figure 2
Detail of a portion of one tube with C—H···S hydrogen-bonding interactions and C—H···π(ring) interactions shown, respectively, by purple and green dashed lines.

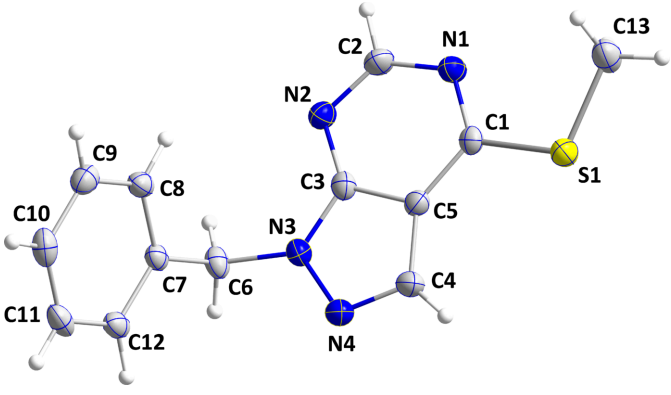

Figure 1
The molecular structure of (I) with the labelling scheme and displacement ellipsoids drawn at the 50% probability level.

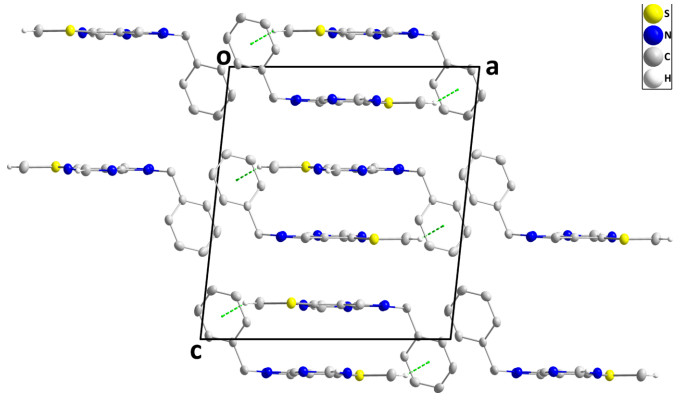

Figure 3
Packing giving an end view of three tubes seen along the *b* axis with C—H···π(ring) interactions shown as dashed lines.

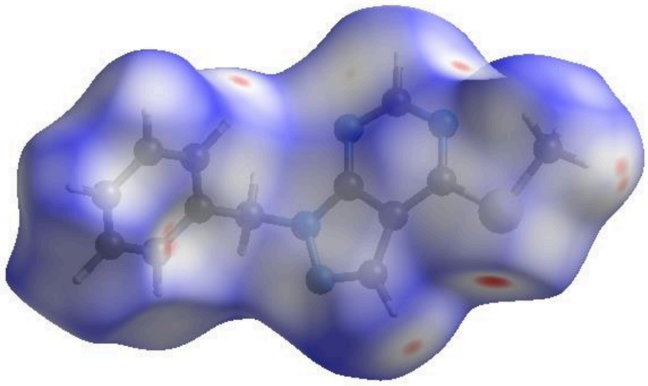

Figure 4
View of the three-dimensional Hirshfeld surface of the title compound plotted over d_{norm}.

4. Hirshfeld surface analysis

In order to visualize the intermolecular interactions in the crystal of (I), a Hirshfeld surface (HS) analysis (Hirshfeld, 1977; Spackman & Jayatilaka, 2009) was carried out by using *CrystalExplorer* (Spackman *et al.*, 2021). In the HS plotted over d_{norm} (Fig. 4), the white surface indicates contacts with distances equal to the sum of van der Waals radii, and the red and blue areas indicate distances shorter (in close contact) or longer (distant contact) than the van der Waals radii, respectively (Venkatesan *et al.*, 2016). The bright-red spots indicate their roles as the respective donors and/or acceptors; they also appear as blue and red regions corresponding to positive and negative potentials on the HS mapped over electrostatic potential (Spackman *et al.*, 2008; Jayatilaka *et al.*, 2005), as shown in Fig. 5. The blue regions indicate positive electrostatic potential (hydrogen-bond donors), while the red regions indicate negative electrostatic potential (hydrogen-bond acceptors). The π–π stacking and C—H$\cdots\pi$ interactions were further visualized by the shape-index surface. This surface can be used to identify characteristic packing modes, in particular,

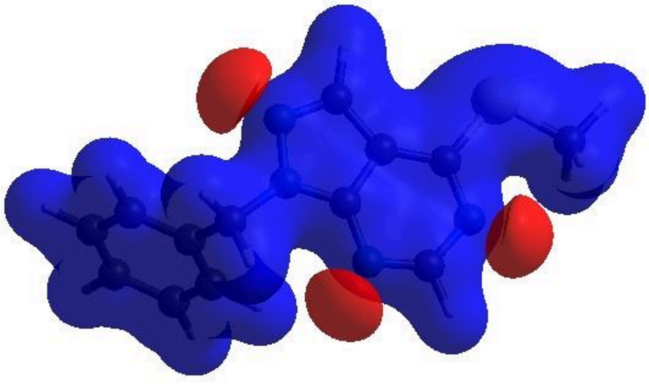

Figure 5
View of the three-dimensional Hirshfeld surface of the title compound plotted over electrostatic potential energy using the STO-3 G basis set at the Hartree–Fock level of theory. Hydrogen-bond donors and acceptors are shown as blue and red regions around the atoms corresponding to positive and negative potentials, respectively.

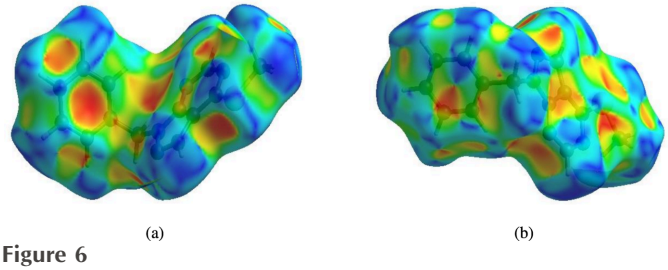

Figure 6
Hirshfeld surface of the title compound plotted over shape-index for two orientations.

planar stacking arrangements and the presence of aromatic stacking interactions. In this regard, the shape-index represents the C—H$\cdots\pi$ interactions as 'red *p*-holes', which are related to the electron ring interactions between the CH groups with the centroid of the aromatic rings of neighbouring molecules. Fig. 6*a* clearly suggests that there are C—H$\cdots\pi$ interactions in (I), and π–π stacking is indicated by the presence of adjacent red and blue triangles (Fig. 6*b*).

The overall two-dimensional fingerprint plot, Fig. 7*a*, and those delineated into H$\cdots$H, H$\cdots$N/N$\cdots$H, H$\cdots$C/C$\cdots$H, H$\cdots$S/S$\cdots$H, C$\cdots$C, C$\cdots$S/S$\cdots$C, N$\cdots$S/S$\cdots$N, C$\cdots$N/N$\cdots$C and N$\cdots$N contacts (McKinnon *et al.*, 2007) are illustrated in Fig. 7*b*–*j*, respectively, together with their relative contribu-

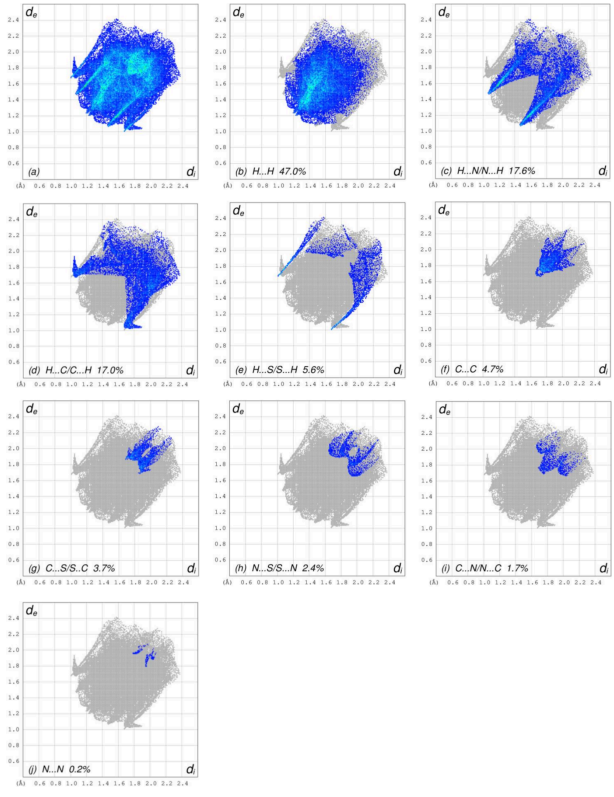

Figure 7
The full two-dimensional fingerprint plots for the title compound, showing (*a*) all interactions, and delineated into (*b*) H$\cdots$H, (*c*) H$\cdots$N/N$\cdots$H, (*d*) H$\cdots$C/C$\cdots$H (*e*) H$\cdots$S/S$\cdots$H, (*f*) C$\cdots$C, (*g*) C$\cdots$S/S$\cdots$C, (*h*) N$\cdots$S/S$\cdots$N, (i) C$\cdots$N/N$\cdots$C and (*j*) N$\cdots$N interactions. The d_i and d_e values are the closest internal and external distances (in Å) from given points on the Hirshfeld surface.

tions to the Hirshfeld surface. The most important interaction is H···H, contributing 47.0% to the overall crystal packing, which is reflected in Fig. 7*b* as widely scattered points of high density due to the large hydrogen content of the molecule with the tip at $d_e = d_i = 1.20$ Å. The symmetrical pair of spikes resulting in the fingerprint plot delineated into H···N/N···H contacts (Fig. 7*c*) with a 17.6% contribution to the HS has the tips at $d_e + d_i = 2.52$ Å. In the presence of C—H···π interactions (Table 1, Fig. 6), the H···C/C···H contacts, contributing 17.0% to the overall crystal packing, are reflected in Fig. 7*d* with the tips at $d_e + d_i = 2.73$ Å. The H···S/S···H contacts (Fig. 7*e*) contribute 5.6% to the HS, and their symmetrical pair of spikes has the tips at $d_e + d_i = 2.68$ Å. The C···C contacts (Fig. 7*f*) have an arrow-shaped distribution of points, contributing 4.7% to the HS, with the tip at $d_e = d_i = 1.68$ Å. The symmetrical pairs of C···S/S···C (Fig. 7*g*) and N···S/S···N (Fig. 7*h*) contacts contribute 3.7% and 2.4% to the HS, and they are observed with the tips at $d_e + d_i = 3.58$ Å and $d_e + d_i = 3.61$ Å, respectively. Finally, the C···N/N···C (Fig. 7*i*) and N···N (Fig. 7*j*) contacts, with 1.7% and 0.2% contributions to the HS, have very low abundance.

The nearest neighbour environment of a molecule can be determined from the colour patches on the HS based on how close to other molecules they are. The Hirshfeld surface representations with the function d_{norm} plotted onto the surface are shown for the H···H, H···N/N···H and H···C/C···H interactions in Fig. 8*a–c*, respectively. The Hirshfeld surface analysis confirms the importance of H-atom contacts in establishing the packing. The large number of H···H, H···N/N···H and H···C/C···H interactions suggest that van der Waals interactions and hydrogen bonding play the major roles in the crystal packing (Hathwar *et al.*, 2015).

5. Crystal voids

The strength of the crystal packing is important for determining the response to an applied mechanical force. For checking the mechanical stability of the crystal, a void analysis was performed by adding up the electron densities of the spherically symmetric atoms comprised in the asymmetric unit (Turner *et al.*, 2011). The void surface is defined as an isosurface of the procrystal electron density and is calculated for the whole unit cell where the void surface meets the boundary of the unit cell and capping faces are generated to create an enclosed volume. The volume of the crystal voids (Fig. 9*a*,*b*) and the percentage of free space in the unit cell are calculated as 76.45 Å^3 and 6.39%, respectively. Thus, the crystal packing appears compact and the mechanical stability should be substantial.

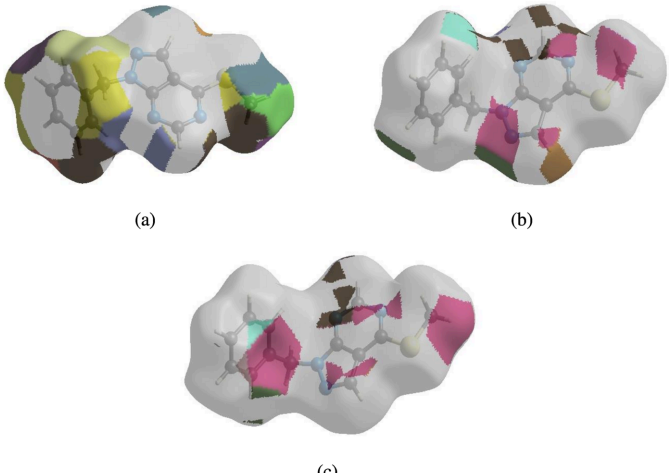

Figure 8
The Hirshfeld surface representations with the fragment patch plotted onto the surface for (*a*) H···H, (*b*) H···N/N···H and (*c*) H···C/C···H interactions.

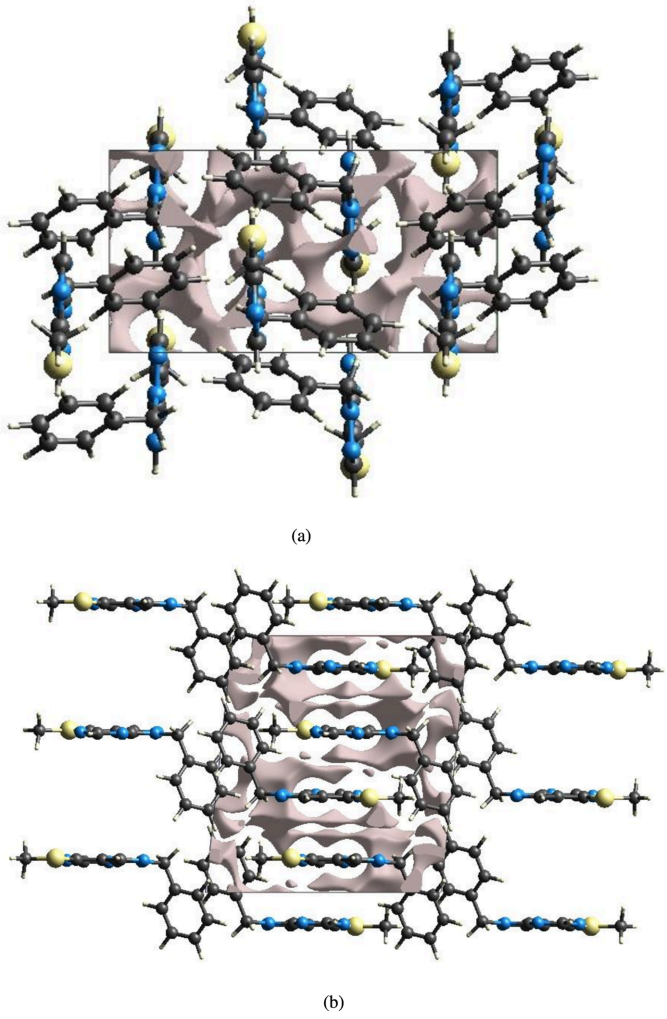

Figure 9
Graphical views of voids in the crystal packing of (I) (*a*) along the *a* axis and (*b*) along the *b* axis. The grey shaded areas represent the filled regions (electron densities), while the colourless regions represent the crystal voids (free spaces).

6. Interaction energy calculations and energy frameworks

The intermolecular interaction energies were calculated using the CE–B3LYP/6–31G(d,p) energy model available in *Crys-*

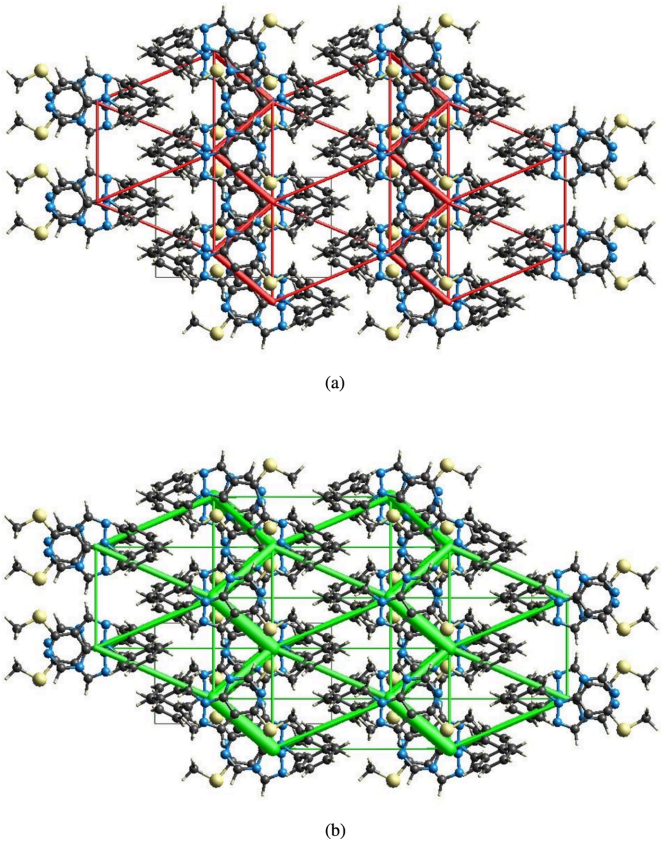

Figure 10
The energy frameworks for a cluster of molecules of (I) viewed down the *c* axis showing (*a*) electrostatic energy and (*b*) dispersion energy diagrams. The cylindrical radius is proportional to the relative strength of the corresponding energies and they were adjusted to the same scale factor of 80 with cut-off value of 5 kJ mol^{-1} within 2×2×2 unit cells.

talExplorer (Spackman *et al.*, 2021), where a cluster of molecules is generated by applying crystallographic symmetry operations with respect to a selected central molecule within the radius of 3.8 Å by default (Turner *et al.*, 2014). The total intermolecular energy (E_{tot}) is the sum of electrostatic (E_{ele}), polarization (E_{pol}), dispersion (E_{dis}) and exchange-repulsion (E_{rep}) energies (Turner *et al.*, 2015) with scale factors of 1.057, 0.740, 0.871 and 0.618, respectively (Mackenzie *et al.*, 2017). Hydrogen-bonding interaction energies (in kJ mol^{-1}) were calculated to be −30.3(E_{ele}), −3.6 (E_{pol}), −74.7 (E_{dis}), 70.9 (E_{rep}) and −55.9 (E_{tot}) for the C2—H2···S1 hydrogen-bonding interaction. Energy frameworks combine the calculation of intermolecular interaction energies with a graphical representation of their magnitude (Turner *et al.*, 2015). Energies between molecular pairs are represented as cylinders joining the centroids of pairs of molecules with the cylinder radius proportional to the relative strength of the corresponding interaction energy. Energy frameworks were constructed for E_{ele} (red cylinders) and E_{dis} (green cylinders) (Fig. 10*a*,*b*). The evaluation of the electrostatic, dispersion and total energy frameworks indicate that the stabilization is dominated *via* the dispersion energy contributions in the crystal structure of (I).

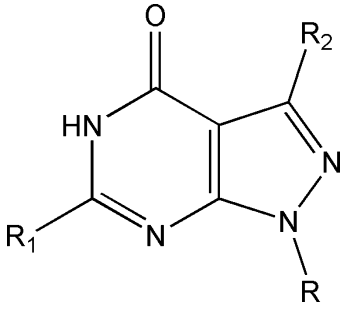

Figure 11
Scheme used for the database search.

7. Database survey

A search of the Cambridge Structural Database (CSD, updated to March 2024; Groom *et al.*, 2016) using the search fragment detailed in Fig. 11 (*R* = C—CH, C—C—OH; R_1 = R_2 = nothing) identified eleven relevant hits. These structures include *R* = *t*-Bu, R_2 = H, R_1 = Ph (RULHEN; Liu *et al.*, 2015), *p*-anis (QIBVIH; Tan *et al.*, 2007); R_2 = H, *R* = *i*-Pr, R_1 = cyclobutanecarboxamido (QIBVON; Tan *et al.*, 2007), *R* = *n*-Bu, R_1 = benzamido (QIBWAA; Tan *et al.*, 2007), *R* = 3-phenylpropyl, R_1= CH_3S (IFICUV; Avasthi *et al.*, 2002), *R* = 2-chloroethyl, R_1= H (XAZRAT; Khazi *et al.*, 2012); *R* = 1-*β*-D-ribofuranosyl, R_1 = H, R_2 = OMe (FOVHIH; Anderson *et al.*, 1986), R_1= NH_2, *R*" = H (YOMJIW; Ren *et al.*, 2019); *R* = 2-deoxy-*β*-D-*erythro*-pentofuranosyl, R_1 = NH_2, R_2 = Br (HIPPAX; Seela *et al.*, 1999), R_2 = I (HIPPEB; Seela *et al.*, 1999); *R* = 2-deoxy-2-fluoro-*β*-D-arabinofuranosyl, R_1= NH_2, R_2= Br (EJEJUY; He *et al.*, 2003). Analysis of the molecular geometries revealed that while the pyrazolopyrimidine unit remained essentially planar as in the molecule of (I), the diversity of substituents in these related structures and the presence of additional hydrogen bonding results in distinctly different crystal packings.

8. Synthesis and crystallization

A catalytic amount of tetra-*n*-butylammonium bromide (0.33 mmol) was added to a solution of 1-benzyl-1*H*-pyrazolo[3,4-d]pyrimidine-4(5*H*)-thione (10 mmol), iodomethane (10 mmol) and potassium carbonate (6.51 mmol) in dimethylformamide (DMF, 40 ml). The mixture was stirred for 24 h. The solid material was removed by filtration and the solvent evaporated *in vacuo*. The resulting colourless solid product was purified by recrystallization from ethanol. Yield: 82%.

9. Refinement

Crystal data, data collection and structure refinement details are summarized in Table 2. Hydrogen atoms were located in difference-Fourier maps and were refined freely.

Table 2
Experimental details.

Crystal data	
Chemical formula	$C_{13}H_{12}N_4S$
M_r	256.33
Crystal system, space group	Monoclinic, $P2_1/c$
Temperature (K)	150
a, b, c (Å)	12.4617 (5), 7.0766 (3), 13.6500 (5)
β (°)	96.085 (1)
V (Å^3)	1196.96 (8)
Z	4
Radiation type	Cu $K\alpha$
μ (mm^{-1})	2.29
Crystal size (mm)	0.26 × 0.22 × 0.16
Data collection	
Diffractometer	Bruker D8 VENTURE PHOTON 100 CMOS
Absorption correction	Multi-scan (*SADABS*; Krause *et al.*, 2015)
T_{min}, T_{max}	0.59, 0.72
No. of measured, independent and observed [$I > 2\sigma(I)$] reflections	8877, 2388, 2292
R_{int}	0.026
(sin $\theta/\lambda)_{max}$ (Å^{-1})	0.626
Refinement	
$R[F^2 > 2\sigma(F^2)]$, $wR(F^2)$, S	0.049, 0.135, 1.10
No. of reflections	2388
No. of parameters	212
H-atom treatment	All H-atom parameters refined
$\Delta\rho_{max}$, $\Delta\rho_{min}$ (e Å^{-3})	0.68, −0.42

Computer programs: *APEX3* and *SAINT* (Bruker, 2016), *SAINT* (Bruker, 2016), *SHELXT/5* (Sheldrick, 2015*a*), *SHELXL2018/3* (Sheldrick, 2015*b*), *DIAMOND* (Brandenburg & Putz, 2012) and *SHELXTL* (Sheldrick, 2008).

Funding information

The support of NSF-MRI grant No. 1228232 for the purchase of the diffractometer and Tulane University for support of the Tulane Crystallography Laboratory are gratefully acknowledged. TH is grateful to Hacettepe University Scientific Research Project Unit (grant No. 013 D04 602 004).

References

Anderson, J. D., Dalley, N. K., Revankar, G. R. & Robins, R. K. (1986). *J. Heterocycl. Chem.* **23**, 1869–1878.
Avasthi, K., Rawat, D. S., Sarkhel, S. & Maulik, P. R. (2002). *Acta Cryst.* C**58**, o325–o327.
Bakavoli, M., Bagherzadeh, G., Vaseghifar, M., Shiri, A., Pordel, M., Mashreghi, M., Pordeli, P. & Araghi, M. (2010). *Eur. J. Med. Chem.* **45**, 647–650.
Brandenburg, K. & Putz, H. (2012). *DIAMOND*, Crystal Impact GbR, Bonn, Germany.
Bruker (2016). *APEX3* and *SAINT*. Bruker AXS, Inc., Madison, Wisconsin, USA.
El-Mekabaty, A. (2015). *Chem. Heterocycl. Compd*, **50**, 1698–1706.
El-Tombary, A. A. (2013). *Sci. Pharm.* **81**, 393–422.
Groom, C. R., Bruno, I. J., Lightfoot, M. P. & Ward, S. C. (2016). *Acta Cryst.* B**72**, 171–179.
Gudmundsson, K. S., Johns, B. A. & Weatherhead, J. (2009). *Bioorg. Med. Chem. Lett.* **19**, 5689–5692.
Hathwar, V. R., Sist, M., Jørgensen, M. R. V., Mamakhel, A. H., Wang, X., Hoffmann, C. M., Sugimoto, K., Overgaard, J. & Iversen, B. B. (2015). *IUCrJ*, **2**, 563–574.
He, J., Eickmeier, H. & Seela, F. (2003). *Acta Cryst.* C**59**, o406–o408.
Hirshfeld, H. L. (1977). *Theor. Chim. Acta*, **44**, 129–138.
Irrou, E., Elmachkouri, Y. A., Oubella, A., Ouchtak, H., Dalbouha, S., Mague, J. T., Hökelek, T., El Ghayati, L., Sebbar, N. K. & Taha, M. L. (2022). *Acta Cryst.* E**78**, 953–960.
Jayatilaka, D., Grimwood, D. J., Lee, A., Lemay, A., Russel, A. J., Taylor, C., Wolff, S. K., Cassam-Chenai, P. & Whitton, A. (2005). *TONTO* - A System for Computational Chemistry. Available at: http://hirshfeldsurface.net/
Kandeel, M. M., Mohamed, L. W., Abd El Hamid, M. K. & Negmeldin, A. T. (2012). *Sci. Pharm.* **80**, 531–545.
Khazi, M. I. A., Fathima, N., Belavagi, N. S., Begum, N. S. & Khazi, I. M. (2012). *Acta Cryst.* E**68**, o2083.
Krause, L., Herbst-Irmer, R., Sheldrick, G. M. & Stalke, D. (2015). *J. Appl. Cryst.* **48**, 3–10.
Liu, M.-X., Li, J. R., Zheng, K., Yao, H., Zhang, Q. & Shi, D.-X. (2015). *Tetrahedron*, **71**, 7658–7662.
Mackenzie, C. F., Spackman, P. R., Jayatilaka, D. & Spackman, M. A. (2017). *IUCrJ*, **4**, 575–587.
Maher, M., Kassab, A. E., Zaher, A. F. & Mahmoud, Z. (2019). *J. Enzyme Inhib. Med. Chem.* **34**, 532–546.
McKinnon, J. J., Jayatilaka, D. & Spackman, M. A. (2007). *Chem. Commun.* pp. 3814–3816.
Ren, H., An, H. & Tao, J. (2019). *Molecules*, **24**, 983.
Sebbar, N. K., Mekhzoum, M. E. M., Essassi, E. M., Zerzouf, A., Talbaoui, A., Bakri, Y., Saadi, M. & Ammari, L. E. (2016). *Res. Chem. Intermed.* **42**, 6845–6862.
Seela, F., Becher, G., Rosemeyer, H., Reuter, H., Kastner, G. & Mikhailopulo, I. A. (1999). *Helv. Chim. Acta*, **82**, 105–124.
Severina, A., Georgiyants, V. A., Shtrygol, S. Y. & Kavraiskyi, D. P. (2016). *Scr. Sci. Pharm.* **3**, 36–40.
Sheldrick, G. M. (2008). *Acta Cryst.* A**64**, 112–122.
Sheldrick, G. M. (2015*a*). *Acta Cryst.* A**71**, 3–8.
Sheldrick, G. M. (2015*b*). *Acta Cryst.* C**71**, 3–8.
Song, X. J., Shao, Y. & Dong, X. G. (2011). *Chin. Chem. Lett.* **22**, 1036–1038.
Spackman, M. A. & Jayatilaka, D. (2009). *CrystEngComm*, **11**, 19–32.
Spackman, M. A., McKinnon, J. J. & Jayatilaka, D. (2008). *CrystEngComm*, **10**, 377–388.
Spackman, P. R., Turner, M. J., McKinnon, J. J., Wolff, S. K., Grimwood, D. J., Jayatilaka, D. & Spackman, M. A. (2021). *J. Appl. Cryst.* **54**, 1006–1011.
Tan, T. M. C., Yang, F., Fu, H., Raghavendra, M. S. & Lam, Y. (2007). *J. Comb. Chem.* **9**, 210–218.
Turner, M. J., Grabowsky, S., Jayatilaka, D. & Spackman, M. A. (2014). *J. Phys. Chem. Lett.* **5**, 4249–4255.
Turner, M. J., McKinnon, J. J., Jayatilaka, D. & Spackman, M. A. (2011). *CrystEngComm*, **13**, 1804–1813.
Turner, M. J., Thomas, S. P., Shi, M. W., Jayatilaka, D. & Spackman, M. A. (2015). *Chem. Commun.* **51**, 3735–3738.
Venkatesan, P., Thamotharan, S., Ilangovan, A., Liang, H. & Sundius, T. (2016). *Spectrochim. Acta A Mol. Biomol. Spectrosc.* **153**, 625–636.
Zhang, C., Zhou, Q., Wu, X. N., Huang, Y. D., Zhou, J., Lai, Z., Wu, Y. & Luo, H. B. (2018). *J. Enzyme Inhib. Med. Chem.* **33**, 260–270.

supporting information

Acta Cryst. (2024). E**80**, 783-788 [https://doi.org/10.1107/S2056989024005954]

Crystal structure determination and analyses of Hirshfeld surface, crystal voids, intermolecular interaction energies and energy frameworks of 1-benzyl-4-(methylsulfanyl)-3a,7a-dihydro-1*H*-pyrazolo[3,4-*d*]pyrimidine

Nour El Hoda Mustaphi, Amina Chlouchi, Mohamed El Hafi, Joel T. Mague, Tuncer Hökelek, Hanae El Monfalouti, Amal Haoudi and Ahmed Mazzah

Computing details

1-Benzyl-4-(methylsulfanyl)-3a,7a-dihydro-1*H*-pyrazolo[3,4-*d*]pyrimidine

Crystal data

$C_{13}H_{12}N_4S$
$M_r = 256.33$
Monoclinic, $P2_1/c$
$a = 12.4617$ (5) Å
$b = 7.0766$ (3) Å
$c = 13.6500$ (5) Å
$\beta = 96.085$ (1)°
$V = 1196.96$ (8) Å^3
$Z = 4$
$F(000) = 536$
$D_x = 1.422$ Mg m^{-3}
Cu $K\alpha$ radiation, $\lambda = 1.54178$ Å
Cell parameters from 7875 reflections
$\theta = 6.3$–$74.7°$
$\mu = 2.29$ mm^{-1}
$T = 150$ K
Block, colourless
0.26 × 0.22 × 0.16 mm

Data collection

Bruker D8 VENTURE PHOTON 100 CMOS diffractometer
Radiation source: INCOATEC IμS micro–focus source
Mirror monochromator
Detector resolution: 10.4167 pixels mm^{-1}
ω scans
Absorption correction: multi-scan (*SADABS*; Krause *et al.*, 2015)
$T_{min} = 0.59$, $T_{max} = 0.72$
8877 measured reflections
2388 independent reflections
2292 reflections with $I > 2\sigma(I)$
$R_{int} = 0.026$
$\theta_{max} = 74.7°$, $\theta_{min} = 6.5°$
$h = -15 \rightarrow 14$
$k = -8 \rightarrow 8$
$l = -15 \rightarrow 17$

Refinement

Refinement on F^2
Least-squares matrix: full
$R[F^2 > 2\sigma(F^2)] = 0.049$
$wR(F^2) = 0.135$
$S = 1.10$
2388 reflections
212 parameters
0 restraints
Primary atom site location: dual
Secondary atom site location: difference Fourier map
Hydrogen site location: difference Fourier map
All H-atom parameters refined
$w = 1/[\sigma^2(F_o^2) + (0.0792P)^2 + 0.9126P]$ where $P = (F_o^2 + 2F_c^2)/3$
$(\Delta/\sigma)_{max} = 0.001$
$\Delta\rho_{max} = 0.68$ e Å^{-3}
$\Delta\rho_{min} = -0.42$ e Å^{-3}
Extinction correction: *SHELXL2018/3* (Sheldrick, 2015*b*), $Fc^* = kFc[1+0.001xFc^2\lambda^3/\sin(2\theta)]^{-1/4}$
Extinction coefficient: 0.0175 (15)

Special details

Geometry. All esds (except the esd in the dihedral angle between two l.s. planes) are estimated using the full covariance matrix. The cell esds are taken into account individually in the estimation of esds in distances, angles and torsion angles; correlations between esds in cell parameters are only used when they are defined by crystal symmetry. An approximate (isotropic) treatment of cell esds is used for estimating esds involving l.s. planes.

Refinement. Refinement of F^2 against ALL reflections. The weighted R-factor wR and goodness of fit S are based on F^2, conventional R-factors R are based on F, with F set to zero for negative F^2. The threshold expression of $F^2 > 2\text{sigma}(F^2)$ is used only for calculating R-factors(gt) etc. and is not relevant to the choice of reflections for refinement. R-factors based on F^2 are statistically about twice as large as those based on F, and R- factors based on ALL data will be even larger.

Fractional atomic coordinates and isotropic or equivalent isotropic displacement parameters (Å²)

	x	*y*	*z*	U_{iso}*/U_{eq}
S1	0.65190 (4)	0.56176 (7)	0.63280 (4)	0.0270 (2)
N1	0.60237 (13)	0.1966 (2)	0.62462 (13)	0.0254 (4)
N2	0.42503 (15)	0.0580 (2)	0.61920 (13)	0.0250 (4)
N3	0.28464 (13)	0.2921 (2)	0.62089 (12)	0.0236 (4)
N4	0.27715 (14)	0.4851 (3)	0.62427 (13)	0.0262 (4)
C1	0.56283 (15)	0.3718 (3)	0.62822 (13)	0.0202 (4)
C2	0.53049 (18)	0.0519 (3)	0.62047 (17)	0.0286 (5)
H2	0.561 (2)	−0.074 (4)	0.618 (2)	0.040 (8)*
C3	0.38820 (15)	0.2371 (3)	0.62210 (13)	0.0217 (4)
C4	0.37631 (17)	0.5524 (3)	0.62805 (15)	0.0250 (4)
H4	0.3872 (18)	0.676 (4)	0.6326 (16)	0.016 (5)*
C5	0.45191 (16)	0.4014 (3)	0.62684 (14)	0.0213 (4)
C6	0.18860 (16)	0.1711 (3)	0.61404 (14)	0.0254 (4)
H6A	0.213 (2)	0.050 (4)	0.6369 (18)	0.024 (6)*
H6B	0.144 (2)	0.215 (4)	0.6594 (18)	0.024 (6)*
C7	0.13101 (14)	0.1627 (3)	0.51110 (13)	0.0204 (4)
C8	0.17719 (16)	0.0661 (3)	0.43709 (15)	0.0232 (4)
H8	0.242 (2)	0.004 (4)	0.4507 (16)	0.021 (5)*
C9	0.12422 (18)	0.0575 (3)	0.34245 (16)	0.0271 (5)
H9	0.156 (2)	−0.003 (4)	0.295 (2)	0.038 (7)*
C10	0.02500 (17)	0.1456 (3)	0.32115 (16)	0.0293 (5)
H10	−0.004 (2)	0.137 (4)	0.264 (2)	0.041 (8)*
C11	−0.02157 (16)	0.2423 (3)	0.39411 (16)	0.0290 (5)
H11	−0.082 (2)	0.299 (4)	0.3801 (19)	0.033 (7)*
C12	0.03167 (15)	0.2506 (3)	0.48894 (15)	0.0245 (4)
H12	−0.003 (2)	0.321 (4)	0.538 (2)	0.041 (7)*
C13	0.77879 (19)	0.4440 (3)	0.6316 (2)	0.0334 (5)
H13A	0.781 (2)	0.381 (4)	0.570 (2)	0.040 (7)*
H13B	0.787 (2)	0.361 (4)	0.686 (2)	0.036 (7)*
H13C	0.836 (3)	0.547 (5)	0.633 (3)	0.068 (11)*

Atomic displacement parameters (Å²)

	U^{11}	U^{22}	U^{33}	U^{12}	U^{13}	U^{23}
S1	0.0236 (3)	0.0230 (3)	0.0341 (3)	0.00000 (17)	0.0021 (2)	−0.00033 (17)

N1	0.0225 (8)	0.0211 (8)	0.0327 (9)	0.0011 (6)	0.0039 (7)	0.0009 (6)
N2	0.0259 (9)	0.0198 (8)	0.0295 (9)	−0.0009 (6)	0.0042 (7)	−0.0002 (6)
N3	0.0194 (8)	0.0252 (9)	0.0260 (8)	−0.0017 (6)	0.0021 (6)	−0.0013 (6)
N4	0.0242 (9)	0.0251 (9)	0.0293 (8)	0.0022 (7)	0.0024 (6)	−0.0034 (7)
C1	0.0211 (9)	0.0214 (9)	0.0178 (8)	−0.0022 (7)	0.0006 (6)	0.0010 (7)
C2	0.0281 (11)	0.0191 (10)	0.0387 (12)	0.0024 (8)	0.0039 (9)	−0.0011 (8)
C3	0.0214 (9)	0.0242 (10)	0.0194 (8)	−0.0034 (7)	0.0018 (7)	−0.0006 (7)
C4	0.0227 (10)	0.0242 (11)	0.0281 (10)	0.0038 (7)	0.0023 (8)	−0.0031 (7)
C5	0.0224 (10)	0.0197 (9)	0.0216 (9)	−0.0003 (7)	0.0012 (7)	−0.0016 (7)
C6	0.0201 (9)	0.0320 (11)	0.0246 (9)	−0.0067 (8)	0.0045 (8)	0.0002 (8)
C7	0.0161 (8)	0.0200 (8)	0.0255 (9)	−0.0029 (7)	0.0036 (7)	0.0010 (7)
C8	0.0190 (10)	0.0216 (9)	0.0294 (10)	0.0004 (7)	0.0047 (8)	0.0002 (7)
C9	0.0302 (11)	0.0250 (10)	0.0272 (10)	−0.0050 (8)	0.0076 (8)	−0.0037 (7)
C10	0.0265 (10)	0.0329 (11)	0.0273 (10)	−0.0099 (8)	−0.0036 (8)	0.0048 (8)
C11	0.0164 (9)	0.0299 (11)	0.0400 (11)	−0.0013 (8)	−0.0008 (8)	0.0082 (9)
C12	0.0187 (9)	0.0219 (9)	0.0337 (10)	−0.0012 (7)	0.0066 (7)	0.0002 (7)
C13	0.0256 (11)	0.0296 (12)	0.0441 (13)	−0.0020 (8)	−0.0003 (9)	0.0039 (9)

Geometric parameters (Å, º)

S1—C1	1.7400 (19)	C6—H6A	0.95 (3)
S1—C13	1.789 (2)	C6—H6B	0.93 (3)
N1—C1	1.337 (3)	C7—C12	1.390 (3)
N1—C2	1.358 (3)	C7—C8	1.394 (3)
N2—C2	1.313 (3)	C8—C9	1.388 (3)
N2—C3	1.350 (3)	C8—H8	0.91 (2)
N3—C3	1.346 (3)	C9—C10	1.388 (3)
N3—N4	1.370 (2)	C9—H9	0.90 (3)
N3—C6	1.466 (2)	C10—C11	1.385 (3)
N4—C4	1.320 (3)	C10—H10	0.83 (3)
C1—C5	1.396 (3)	C11—C12	1.392 (3)
C2—H2	0.97 (3)	C11—H11	0.86 (3)
C3—C5	1.406 (3)	C12—H12	0.97 (3)
C4—C5	1.426 (3)	C13—H13A	0.96 (3)
C4—H4	0.89 (2)	C13—H13B	0.95 (3)
C6—C7	1.510 (3)	C13—H13C	1.02 (4)
C1—S1—C13	101.59 (10)	C7—C6—H6B	111.9 (15)
C1—N1—C2	117.19 (17)	H6A—C6—H6B	106 (2)
C2—N2—C3	111.93 (17)	C12—C7—C8	119.25 (18)
C3—N3—N4	110.87 (16)	C12—C7—C6	120.62 (17)
C3—N3—C6	127.36 (18)	C8—C7—C6	120.13 (17)
N4—N3—C6	121.74 (16)	C9—C8—C7	120.25 (19)
C4—N4—N3	107.11 (16)	C9—C8—H8	119.2 (14)
N1—C1—C5	120.45 (17)	C7—C8—H8	120.5 (14)
N1—C1—S1	118.78 (15)	C10—C9—C8	120.03 (19)
C5—C1—S1	120.76 (15)	C10—C9—H9	121.0 (18)
N2—C2—N1	129.09 (19)	C8—C9—H9	119.0 (18)

N2—C2—H2	115.3 (18)	C11—C10—C9	120.2 (2)
N1—C2—H2	115.6 (18)	C11—C10—H10	123 (2)
N3—C3—N2	126.83 (18)	C9—C10—H10	117 (2)
N3—C3—C5	107.31 (18)	C10—C11—C12	119.65 (19)
N2—C3—C5	125.86 (18)	C10—C11—H11	119.8 (18)
N4—C4—C5	110.24 (18)	C12—C11—H11	120.5 (18)
N4—C4—H4	119.6 (15)	C7—C12—C11	120.61 (19)
C5—C4—H4	130.1 (15)	C7—C12—H12	121.6 (17)
C1—C5—C3	115.47 (18)	C11—C12—H12	117.8 (17)
C1—C5—C4	140.06 (19)	S1—C13—H13A	109.4 (17)
C3—C5—C4	104.47 (17)	S1—C13—H13B	107.5 (17)
N3—C6—C7	112.75 (15)	H13A—C13—H13B	113 (3)
N3—C6—H6A	105.8 (16)	S1—C13—H13C	106 (2)
C7—C6—H6A	112.1 (15)	H13A—C13—H13C	105 (3)
N3—C6—H6B	107.8 (15)	H13B—C13—H13C	115 (3)

C3—N3—N4—C4	−0.3 (2)	N3—C3—C5—C1	−179.69 (16)
C6—N3—N4—C4	−178.65 (17)	N2—C3—C5—C1	0.2 (3)
C2—N1—C1—C5	−0.5 (3)	N3—C3—C5—C4	−0.1 (2)
C2—N1—C1—S1	−179.60 (15)	N2—C3—C5—C4	179.84 (18)
C13—S1—C1—N1	−0.32 (18)	N4—C4—C5—C1	179.4 (2)
C13—S1—C1—C5	−179.38 (17)	N4—C4—C5—C3	−0.1 (2)
C3—N2—C2—N1	0.3 (3)	C3—N3—C6—C7	−99.9 (2)
C1—N1—C2—N2	0.2 (3)	N4—N3—C6—C7	78.2 (2)
N4—N3—C3—N2	−179.71 (18)	N3—C6—C7—C12	−108.9 (2)
C6—N3—C3—N2	−1.4 (3)	N3—C6—C7—C8	71.1 (2)
N4—N3—C3—C5	0.2 (2)	C12—C7—C8—C9	−0.2 (3)
C6—N3—C3—C5	178.49 (16)	C6—C7—C8—C9	179.77 (18)
C2—N2—C3—N3	179.36 (19)	C7—C8—C9—C10	0.1 (3)
C2—N2—C3—C5	−0.6 (3)	C8—C9—C10—C11	0.0 (3)
N3—N4—C4—C5	0.2 (2)	C9—C10—C11—C12	0.0 (3)
N1—C1—C5—C3	0.3 (3)	C8—C7—C12—C11	0.2 (3)
S1—C1—C5—C3	179.39 (13)	C6—C7—C12—C11	−179.80 (18)
N1—C1—C5—C4	−179.1 (2)	C10—C11—C12—C7	−0.1 (3)
S1—C1—C5—C4	0.0 (3)		

Hydrogen-bond geometry (Å, º)

*Cg*3 is the centroid of the C7–C12 phenyl ring.

D—H···*A*	*D*—H	H···*A*	*D*···*A*	*D*—H···*A*
C2—H2···S1^{i}	0.97 (3)	2.81 (3)	3.781 (2)	174 (2)
C13—H13*C*···*Cg*3^{ii}	1.02 (4)	2.49 (4)	3.455 (2)	157 (3)

Symmetry codes: (i) *x*, *y*−1, *z*; (ii) −*x*+1, −*y*+1, −*z*+1.